Journal of Sound and Vibration 329 (2010) 2337–2348

Contents lists available at ScienceDirect

Journal of Sound and Vibration

journal homepage: www.elsevier.com/locate/jsvi

Reference-free crack detection using transfer impedances

Seunghee Park [a], Changgil Lee [b], Hoon Sohn [b,*]

[a] Department of Civil and Environmental Engineering, Sungkyunkwan University, 300 Cheoncheon-dong, Jangan-gu, Suwon, Gyeonggi 440-746, Republic of Korea
[b] Department of Civil and Environmental Engineering, KAIST, 373-1 Guseong-dong, Yuseong-gu, Daejeon 305-701, Republic of Korea

ARTICLE INFO

Article history:
Accepted 5 April 2009
The peer review of this article was organized by the Guest Editor
Available online 14 May 2009

ABSTRACT

A new concept of reference-free damage detection methodology is developed using transfer impedances to detect crack damage in a plate-like structure without using previously collected baseline data. Conventional impedance-based damage detection techniques have been shown to be vulnerable to other types of changes such as temperature variation that may not be relevant to defects of interest. One of the potential disadvantages of the conventional techniques is frequent false-alarms due to these undesirable variations that may occur in field applications. In order to reduce these false-alarms, this paper proposes a new methodology that utilizes transfer impedances obtained between two pairs of collocated PZT patches instead of the electromechanical impedance obtained at one PZT patch. The proposed technique utilizes Lamb mode conversion effects caused by the presence of crack damage in plate structures. Furthermore, an instantaneous damage classification is carried out by comparing mode conversion energy among several combinations of measured signals without any user-specified threshold or relying on the baseline data. The feasibility of the proposed reference-free methodology using transfer impedances is investigated via a series of experiments conducted on an aluminum plate.

1. Introduction

Conventional structural health monitoring (SHM) techniques have focused on schemes where baseline signals are measured so that changes from the baseline can be detected and related to structural defects [1]. However, there are significant technical challenges to realizing this pattern comparison. For instance, structural defects typically take place long after the initial baseline collected, and other operational and environmental variations of the system can produce significant changes in the measured responses, masking potential signal changes due to structure defects [2]. To overcome the drawbacks of the conventional SHM techniques, some reference-free schemes that do not rely on the previously obtained baseline data have been proposed for damage detection in a structure [3–6]. In particular, Kim and Sohn [6] proposed a reference-free scheme based on the fact of that mode conversion due to crack formation can be instantly detected by examining measured Lamb wave signals in the time-domain for crack detection in a plate-like structure with a uniform thickness. This technique requires extraction and identification of individual Lamb wave modes such as symmetric, anti-symmetric and converted modes. However, isolation of these individual modes can be a challenging task due to existence of multiple reflections and overlaps among different Lamb wave modes. In this study, the previous time-domain reference-free technique is advanced by detecting the presence of mode conversion in the

* Corresponding author. Tel.: +82 42 350 3625; fax: +82 42 350 5665.
E-mail address: hoonsohn@kaist.ac.kr (H. Sohn).

0022-460X/$ - see front matter © 2009 Elsevier Ltd. All rights reserved.
doi:10.1016/j.jsv.2009.04.010

frequency-domain using transfer impedances. The proposed frequency-domain technique is developed based on the premise that the energy content of crack-induced mode conversion can be estimated and the mode conversion can be detected when its energy level exceeds the background noise level. Because this improved reference-free technique is based solely on the estimated energy of the converted Lamb modes, crack can be successfully identified regardless of their orientation, location, or number.

This paper is organized as follows. First, the theoretical background for the extraction of crack-induced mode conversion using the PZT polarization direction on Lamb wave generation and measurement are described. Then, the time-domain reference-free damage diagnosis technique previously proposed by our research team is reviewed. Third, a new concept of the frequency-domain reference-free technique is developed using transfer impedances. Furthermore, a damage classification technique is proposed based on the premise that the energy level of the crack-induced mode conversion is always higher than that of the initial errors caused by variations of PZT size, bonding condition and alignment. Finally, the applicability of the proposed reference-free methodology to crack detection is investigated via a series of experiments conducted on an aluminum plate under a laboratory setting.

2. Theoretical backgrounds

2.1. PZT poling characteristic-based mode conversion extraction

Piezoelectric materials develop an electrical charge or voltage when a mechanical pressure is applied. Conversely, they produce deformation (strain) when exposed to an applied electric field. Due to this unique nature of the piezoelectric materials (“piezoelectricity”), they are commonly used for sensing and actuation applications. The overall behavior of the piezoelectric materials as well as their electrical characteristics is governed by the poling direction of the material [7,8]. One of the most widely used piezoelectric materials is lead zirconate titanate (PZT). It has been reported that PZT materials can be very effectively utilized for exciting and measuring guided Lamb wave propagations for SHM applications [9]. If Lamb waves propagating along a thin plate with a uniform thickness encounter a discontinuity such as a sudden thickness change of the plate, some portion of the waves are reflected at the discontinuity point and others are transmitted through it. When a S_0 mode arrives at the discontinuity, the transmitted wave is separated into S_0 and A_0 modes (denoted as S_0/S_0 and A_0/S_0, respectively). In a similar manner, an A_0 mode is also divided into S_0 and A_0 modes (S_0/A_0 and A_0/A_0). Furthermore, the reflected waves at the discontinuity are also converted and split into S_0 and A_0 modes. This phenomenon is called mode conversion [10].

Kim and Sohn [6] has shown that the relative phases among measured Lamb wave modes change according to (1) the side of the PZT patch placement (top or bottom surface), (2) the PZT poling direction and (3) the deformed shape of Lamb waves (symmetric or anti-symmetric) as displayed in Fig. 1. Herein, it is assumed that a narrowband tone-burst signal is applied as an input, and a driving frequency is chosen such that only the fundamental symmetric (S_0) and asymmetric (A_0) modes are generated [11]. Figs. 1(a) and (c) present the relative phase information among Lamb wave modes measured

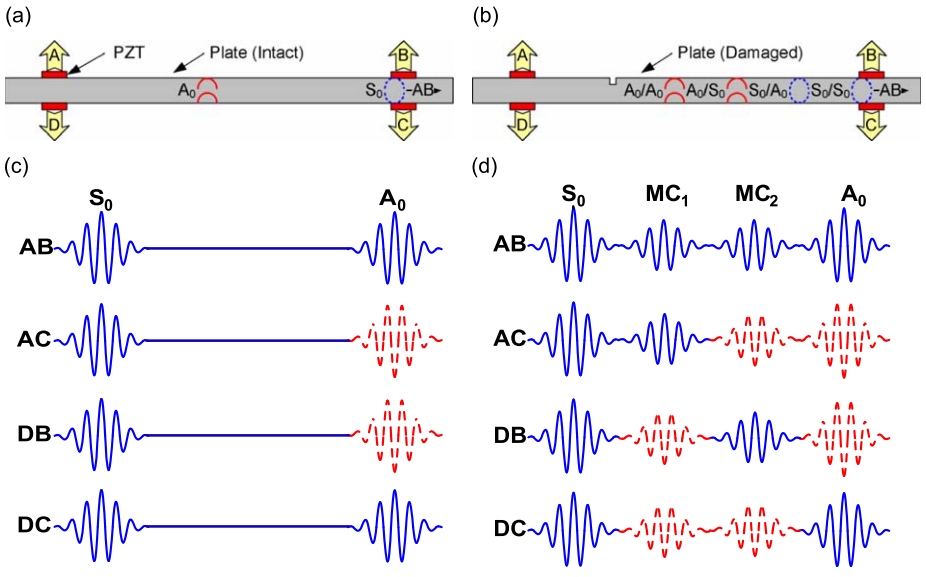

Fig. 1. Comparison of signals obtained from the undamaged and damaged conditions: (a) intact case (without a notch); (b) damaged case (with a notch); (c) signals without a notch; and (d) signals with a notch.

from an intact case while Figs. 1(b) and (d) illustrate a damaged case with a notch. It is noted that the signs of the fundamental (non-converted) modes (S_0 and A_0) are not affected by crack formation. On the other hand, the signs of newly generated (converted) modes (A_0/S_0 and S_0/A_0) are altered depending on the characteristics of a discontinuity that the launching Lamb mode is passing through. When the plate is in a pristine condition, it is observed that signal AB (or AC) becomes identical to signal DC (or DB), as shown in Fig. 1(c). When a crack is formed between PZTs A and B (or PZTs D and C) as shown in Fig. 1(d), signal AB (or AC) is no longer identical to signal DC (or DB) due to different phases among the converted modes.

In Fig. 1(d), the first and second arrivals of the converted modes are defined as MC_1 and MC_2, respectively. Note that MC_1 and MC_2 could be either S_0/A_0 or A_0/S_0 modes depending on the relative position of the crack with respect to the actuating and sensing PZTs. For instance, MC_1 in signal AB becomes a S_0/A_0 mode when the notch is closer to PZT A than B. This is because the S_0/A_0 mode arrives at PZT B earlier than the A_0/S_0 mode. Similarly, MC_2 in signal AB represents the A_0/S_0 mode. Here, the signs of the MC_1 and MC_2 modes in signal AB are assumed to be positive so that the relative phases of the MC_1 and MC_2 modes in other signals (signals AC, DB and DC) can be compared with. For instance, it is shown in Fig. 1(d) that the MC_1 and MC_2 modes in signal DC are out-of-phase when compared with the converted modes in signal AB. On the other hand, the S_0 and A_0 modes in signal DC are identical to the corresponding fundamental modes in signal AB. Therefore, the mode conversions (MC_1 and MC_2 modes) can be extracted simply by subtracting signal DC from signal AB (see Fig. 2(a)). Similarly, the converted modes can be isolated by subtracting signal DB from signal AC (see Fig. 2(b)). Based on these observations, it can be concluded that additional converted modes (MC_1 and MC_2) generated by a notch can be simply extracted by subtracting signal DC from signal AB (or by subtracting signal DB from signal AC). Here, the difference is that the MC_1 and MC_2 modes are in-phase in Fig. 2(a) while they are out-of-phase in Fig. 2(b).

2.2. Decomposition of individual Lamb wave modes from measured time signals

By investigating the relative phase information among the Lamb wave modes measured from the damaged case in Fig. 1(d), the relationship between the measured time signals (signals AB, AC, DB, and DC) and the individual Lamb signals (signals S_0, MC_1, MC_2, and A_0) can be obtained as follows:

$$\begin{bmatrix} \text{Signal AB} \\ \text{Signal AC} \\ \text{Signal DB} \\ \text{Signal DC} \end{bmatrix} = \begin{bmatrix} 1 & 1 & 1 & 1 \\ 1 & 1 & -1 & -1 \\ 1 & -1 & 1 & -1 \\ 1 & -1 & -1 & 1 \end{bmatrix} \times \begin{bmatrix} \text{Signal } S_0 \\ \text{Signal } MC_1 \\ \text{Signal } MC_2 \\ \text{Signal } A_0 \end{bmatrix} \tag{1}$$

Eq. (1) illustrates how different combinations of individual Lamb mode signals constitute each measured signals. The inverse of Eq. (1) shows how each individual Lamb mode signals can be extracted from the measured signals:

$$\begin{bmatrix} \text{Signal } S_0 \\ \text{Signal } MC_1 \\ \text{Signal } MC_2 \\ \text{Signal } A_0 \end{bmatrix} = \frac{1}{4} \begin{bmatrix} 1 & 1 & 1 & 1 \\ 1 & 1 & -1 & -1 \\ 1 & -1 & 1 & -1 \\ 1 & -1 & -1 & 1 \end{bmatrix} \times \begin{bmatrix} \text{Signal AB} \\ \text{Signal AC} \\ \text{Signal DB} \\ \text{Signal DC} \end{bmatrix} \tag{2}$$

Eqs. (1) and (2) are obtained based on the assumption that all PZT patches are identical and PZTs A and D (or PZTs B and C) are perfectly collocated. In reality, these assumptions may not be fully satisfied because of variations in PZT sizes, alignment and bonding conditions. It is noted that these variations in PZTs may generate initial errors between signals AB and DC (or signals AC and DB) even in the absence of cracks.

2.3. Time-domain reference-free damage diagnosis technique

To tackle this issue, Kim and Sohn [6] demonstrated that a threshold value for damage detection can be set as the maximum absolute amplitude of error signals in each decomposed Lamb modes signals. They developed a time-domain

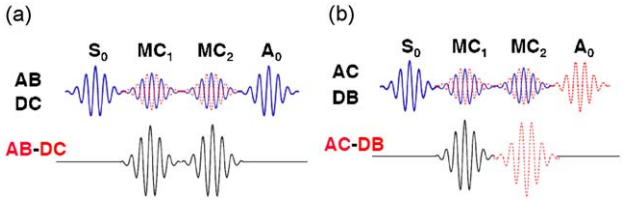

Fig. 2. Extraction of crack-induced mode conversions by subtracting measured time signals: (a) mode conversions obtained by subtracting signal DC from signal AB and (b) mode conversions obtained by subtracting signal DB from signal AC.

reference-free damage detection scheme based on the premise that the crack-induced mode conversions can be extracted from the measured signals (signals AB, AC, DB and DC) and isolated from each other. However, when a crack is not along the direct wave path between the exciting and sensing PZTs (between PZTs A and B (or PZTs D and C)), identification and isolation of mode conversion in the time-domain become difficult. Furthermore, the problem becomes more sophisticated when there are multiple reflections that might overlap with these converted modes due to complex structural geometries.

3. Transfer impedance-based reference-free technique

To overcome the limitation of the aforementioned time-domain approach, this study proposes a transfer impedance-based reference-free technique, which compares only the relative energy of crack-induced mode conversion among four different signal compositions obtained from the measured signals in the frequency-domain. Note that the proposed technique still seeks the additional Lamb mode conversions (MC_1 and MC_2) caused by the presence of crack damage explained in the previous section.

3.1. Composition of mode conversion signals from measured time signals

As mentioned in Section 2.1, the mode conversions (MC_1 and MC_2) generated by a notch can be easily extracted by (1) subtracting signal DC from signal AB or (2) subtracting signal DB from signal AC. Note that the MC_1 modes in signals (AB−DC) and (AC−DB) are in-phase, while the MC_2 modes are fully out-of-phase. Then, MC_1 and MC_2 modes can be further isolated from signals (AB−DC) and (AC−DB) through their summation or subtraction, respectively. Finally, four kinds of composed signals (M1, M2, M3 and M4) can be defined as follows: (1) signal M1 given by $(AB-DC)/2$: contains MC_1 and MC_2; (2) signal M2 given by $(AC-DB)/2$: contains MC_1 and MC_2; (3) signal M3 given by $\{(AB-DC)+(AC-DB)\}/4$: contains only MC_1; and (4) signal M4 given by $\{(AB-DC)-(AC-DB)\}/4$: contains only MC_2. Note that signals M1–M4 are normalized so that MC_1 and MC_2 modes in all composed signals have the same amplitude. These composed signals can be classified into Class A that contains both mode conversions (MC_1 and MC_2) and Class B that includes only one mode conversion (MC_1 or MC_2): The first two (M1 and M2) and the last two (M3 and M4) belong to Classes A and B, respectively, as displayed in Fig. 3. In Fig. 3, the compositions of signals M1–M4 are illustrated assuming that there are only two mode conversions (MC_1 and MC_2) for simplicity. In reality, these compositions can be generalized even when there are multiple mode conversions. The existence of multiple mode conversions occurs (1) when a long time signal with reflections of these converted modes from boundaries is considered and (2) when higher modes are excited at a certain driving frequency. Regardless of the existence of multiple mode conversions, the converted modes can be divided into two categories: ones converted from symmetric modes to anti-symmetric modes and the others transformed from anti-symmetric modes to symmetric modes. They are always generated in pairs. Once we denote these two types of mode conversions as MC_1 and MC_2, the rest of the composition operations can proceed as before.

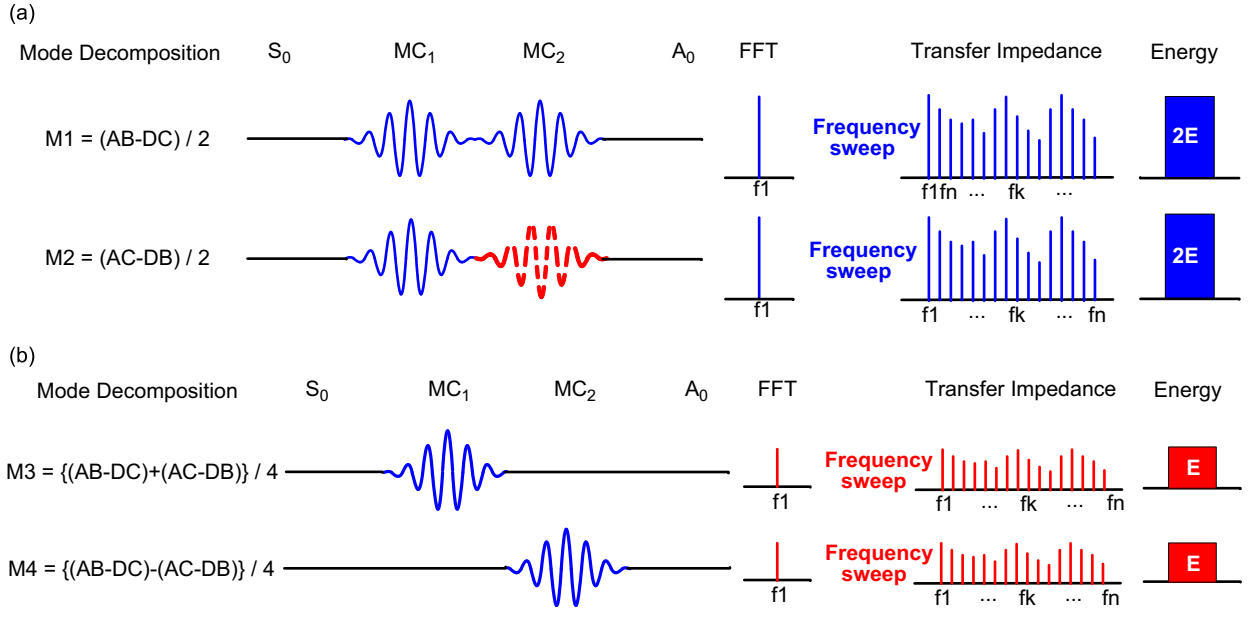

Fig. 3. Transfer impedances of composed mode conversion signals M1–M4: (a) Class A: contains both mode conversions (MC_1 and MC_2) and (b) Class B: contains only one mode conversion (MC_1 or MC_2) (it can be shown that the average energy levels of Class A transfer impedances (for M1 and M2) are approximately twice of these of Class B transfer impedances (for M3 and M4)).

3.2. Calculation of transfer impedances of composed signals M1, M2 M3 and M4

In this subsection, the transfer-impedances are calculated from the composed signals (M1–M4). Here, a transfer impedance is defined as the frequency-response-function (FRF) between a pair of PZT patches (one for 'input' and the other for 'output') while the driving frequency is swept. To evaluate the level of the mode conversions produced by a crack, the energy contents of the composed signals M1–M4 averaged over a certain frequency band have been computed. First, the FRF is obtained through the fast fourier transform (FFT) of the composed signals (M1–M4) at a given driving frequency. Then, the same procedure is repeated over a specified frequency band to obtain transfer impedances. Finally, the total energy of each signal is computed by summing the magnitudes of its FRFs over the entire frequency range investigated. Fig. 3 presents that the transfer impedances of the composed signals have a specific energy-ratio of '2:1' between Class A and Class B signals in a damaged condition. However, it should be noted that the energy ratio will not be always perfectly 2–1. For instance, the MC_1 and MC_2 modes in signal M2 can be fully overlapped and then the corresponding energy can be zero. On the other hand, it is expected that when there exist only initial errors (no mode conversions) in a healthy condition, the energy ratio between Classes A and becomes arbitrary.

3.3. Development of an instantaneous damage classifier

Based on the findings above, a damage classifier that operates on transfer impedance energy is developed in this study. The objective here is to determine the existence of damage (or mode conversion) solely based on the signals measured from the current state of the structure. Often damage classification requires establishment of a threshold value (for unsupervised learning) or a decision boundary (for supervised learning) based on previously obtained baseline data or training data set. However, it has been shown that such dependences on the baseline data can produce frequent false indications of damage. As mentioned previously, the energy ratio between the transfer impedances in Classes A and B would not be exactly 2–1. However, it is expected that the transfer impedance energy of signals M1 and M2 in Class A be certainly larger than those of signals M3 and M4 in Class B in the presence of mode conversion. Based on this observation, the following damage classification statement can be established:

"If the minimum of out-of-class energy differences is larger than the maximum of within-class energy differences, a crack exists. Otherwise, there is no crack".

The minimum of out-of-class energy differences and the maximum of within-class energy differences are defined as $\{\min(X1, X2) - \max(X3, X4)\}$ and $\max(|X1-X2|, |X3-X4|)$, respectively. Here, $X1$–$X4$ denote the mean values of the transfer impedance energy computed for signals M1–M4 over the inspected frequency band, respectively. The maximum of within-class energy differences represents the maximum level of the initial errors, and the minimum of out-of-class energy differences denotes the minimum level of the energy increases due to crack-induced mode conversion. That is, this damage classifier identifies crack formation if the crack-induced mode conversion produces mode conversion energy larger than energy variation due to the initial errors.

In the previous time-domain approach, an optimal driving frequency needs to be selected after examining a Lamb wave tuning curve [12–14]. Furthermore, it is necessary to decompose individual Lamb wave modes such as S_0, A_0 and converted modes in the time-domain. However, this decomposition can be complicated when there are additional higher modes and multiple reflections. On the other hand, the proposed frequency-domain approach does not require the selection of a single optimal driving frequency or decomposition of individual Lamb modes since it only considers the crack-induced energy increase throughout the overall frequency range. Furthermore, since only the overall energy increase produced by mode conversion is of concern, the length of each time signal used for the transfer impedance calculation can be chosen arbitrarily without significantly altering the results. Therefore, it is expected that the proposed frequency-domain approach be more effective than the previous time-domain approach, particularly for structures with complex boundaries.

4. Experimental study

To verify the effectiveness of the proposed frequency-domain approach, an experimental study was carried out. The overall test configuration is shown in Fig. 4. The data acquisition system consists of an arbitrary waveform generator (AWG), a high-speed signal digitizer (DIG), a low noise preamplifier (LNP) and a multiplexer, as shown in Fig. 4(a). A pitch-catch test was performed using a pair of PZT (actuator–sensor) patches attached to a specimen. Using the 16-bits AWG, a tone-burst signal with a ± 10 peak-to-peak voltage was generated, and a driving frequency to the excitation PZT patch was varied from 100 to 200 kHz with an increment of 1 kHz. Then, the PZT patch generated elastic Lamb waves on the specimen, and the response was measured at the other sensing PZT patch. The measured voltage output was amplified by the LNP with a gain of 20 and measured by the 14-bits DIG. In order to improve the signal-to-noise ratio, the pitch-catch signals were measured 10 times and averaged in the time-domain. An aluminum plate with a dimension of $610 \times 400 \times 6\,mm^3$ was tested in this study. Four identical PSI-5AE type PZT patches ($10 \times 10 \times 0.508\,mm^3$) were mounted on both sides of the specimen as shown in Fig. 4(b). PZTs A and D were collocated and attached on the opposite sides of the plate and PZTs B and C were mounted in a similar manner. The arrows denote the positive polling direction of each PZT patch. An intact case

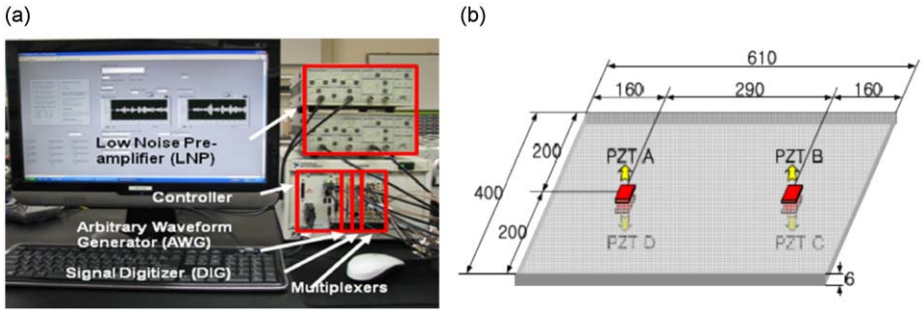

Fig. 4. Experimental setup: (a) data acquisition system and (b) test specimen: an aluminum plate-unit in mm (the arrows denote the positive polling direction of each PZT patch).

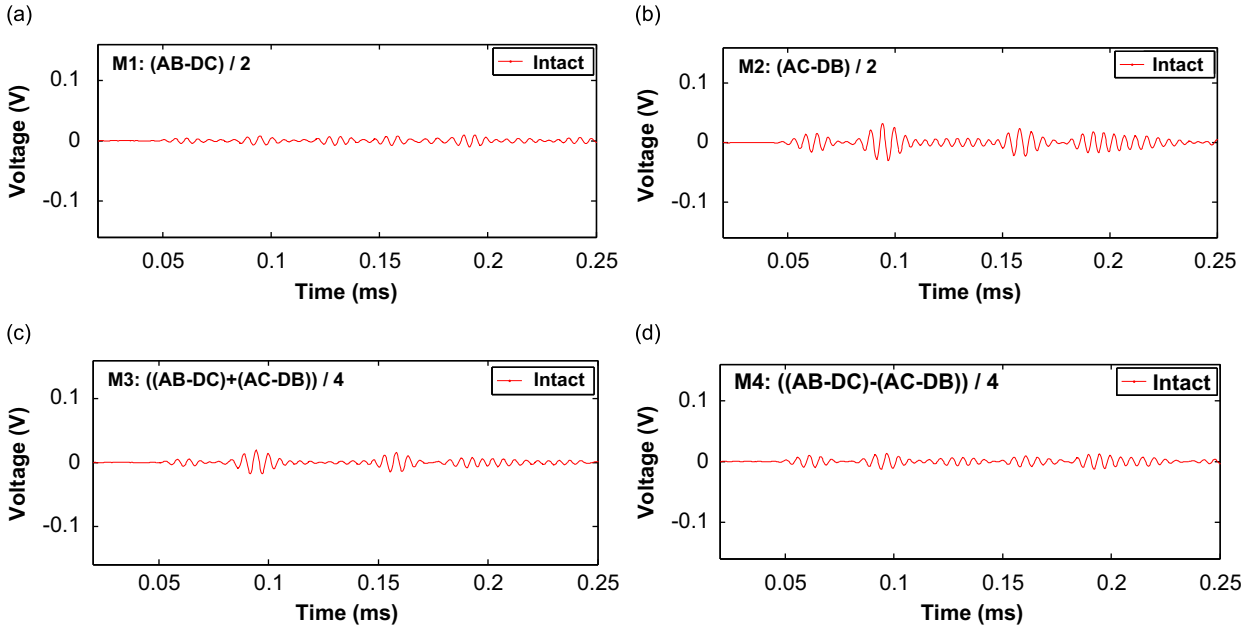

Fig. 5. Signals M1–M4 obtained from the pristine condition of the plate at a driving frequency of 180 kHz: (a) signal M1 given by (AB − DC)/2; (b) signal M2 given by (AC − DB)/2; (c) signal M3 given by {(AB − DC) + (AC − DB)}/4; and (d) signal M4 given by {(AB − DC) − (AC − DB)}/4 (all of these signals are supposed to be null signals in theory, but initial errors due to measurement noise and PZT variations appear in practice).

(without a notch) and four different damage cases with varying notch locations, orientations and numbers were investigated.

4.1. Undamaged case

First, initial data were collected from the pristine condition of the specimen by varying the driving frequency from 100 to 200 kHz with an increment of 1 kHz. Then, the composition of signals M1–M4 described in Section 3.1 was carried out. Fig. 5 shows the composed signals M1–M4 obtained from the initial state of the plate at a driving frequency of 180 kHz. As mentioned earlier, ideally they should be zero for the entire length of the signals in the absence of damage. However, due to the PZT imperfections or measurement noises, some initial errors are observed in these signals.

Then, the transfer impedances shown in Fig. 6(a) were obtained by taking FFT of signals M1–M4 while sweeping the driving frequency from 100 to 200 kHz with an increment of 1 kHz. Then, the transfer impedance energies of the composed signals (M1–M4) were averaged over the entire frequency band in Fig. 6(b). Then, the minimum of out-of-class differences (Diff1) and the maximum of within-class differences (Diff2) defined in Section 3.3 were computed in Fig. 6(c). Since 'Diff 1' is smaller than 'Diff 2', it can be stated that the plate does not have a crack that produces mode conversion beyond initial errors and the condition of the specimen can be instantaneously diagnosed as "healthy condition". Next, four different

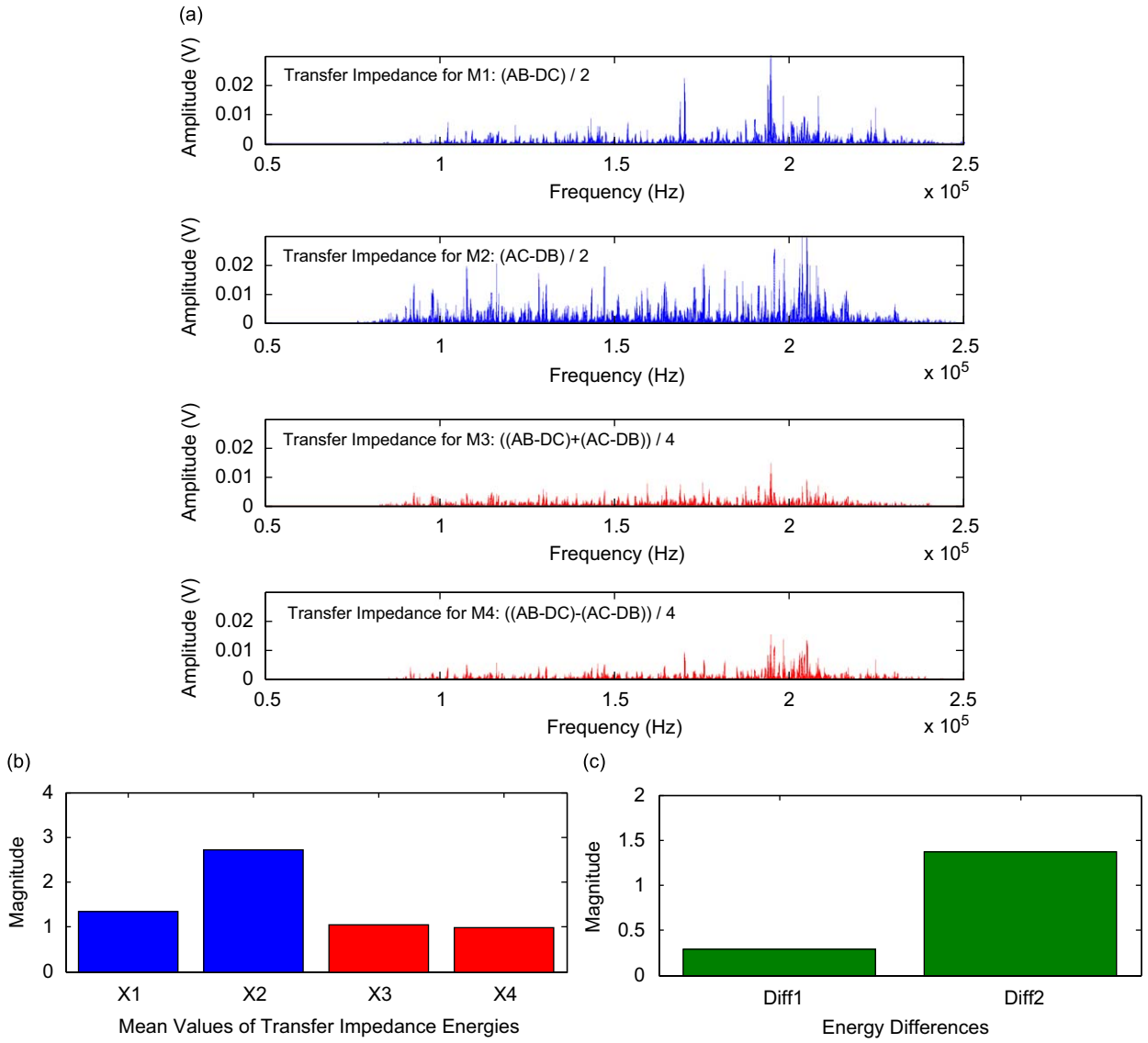

Fig. 6. Instantaneous damage diagnosis using the averaged transfer impedance energies of signals M1–M4 obtained from the intact condition: (a) transfer impedances of signals M1–M4 obtained from the intact condition of the plate; (b) averaged transfer impedance energies ($X1$, $X2$, $X3$ and $X4$) of signals M1–M4; and (c) since Diff 1 < Diff 2, the plate is diagnosed as in its pristine condition.

damage cases shown in Fig. 7 have been investigated (Damage Case I: crack along direct wave propagation path; Damage Case II: crack behind one of the PZTs; Damage Case III: crack out of direct wave path; and Damage Case IV: multiple cracks).

4.2. *Damage Case I: crack along the direct wave propagation path*

For Damage Case I shown in Fig. 7(a), a crack with 40 mm in length, 1 mm in width, and 3 mm in depth was introduced along the direct guided wave propagation path between PZTs A and B and closer to PZT A (60 mm apart from PZT A). It is expected that two converted modes, MC_1 and MC_2 due to the crack damage may occur between the fundamental modes, S_0 and A_0 in the forwarding signal AB. Here, MC_1 denotes the S_0/A_0 mode and the MC_2 does the A_0/S_0 mode, since the crack is closer to PZT A and the S_0 mode travels faster than the A_0 mode. The signals M1–M4 obtained at an excitation frequency of 180 kHz are shown in Fig. 8 and compared with the ones from the intact case. As expected, the appearance of two converted modes (MC_1 and MC_2) are clearly shown between the arrival times of the S_0 and A_0 modes in signals M1 and M2, while only either MC_1 or MC_2 appears in signals M3 and M4 within the same time segment. However, it should

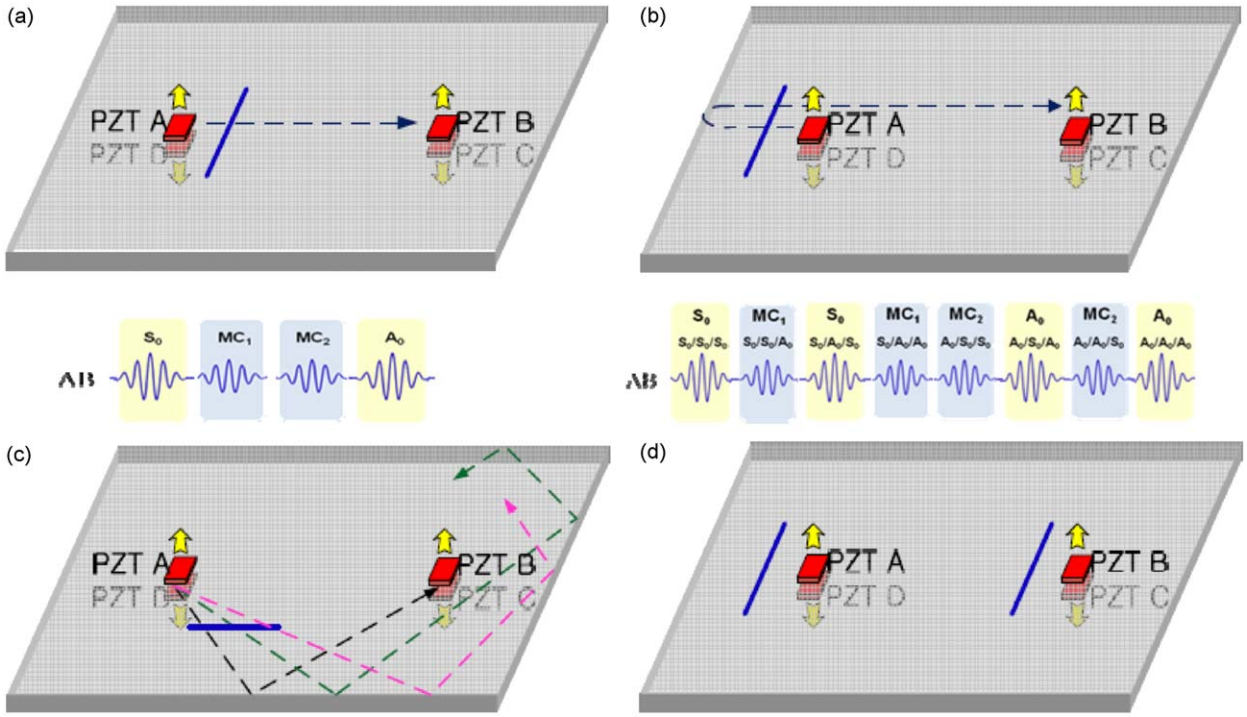

Fig. 7. Four different damage cases investigated in this study: (a) Damage Case I; (b) Damage Case II; (c) Damage Case III; and (d) Damage Case IV (in Figs. (c) and (d), time signals are omitted because each mode conversions and reflections are complicated to identify in the time-domain).

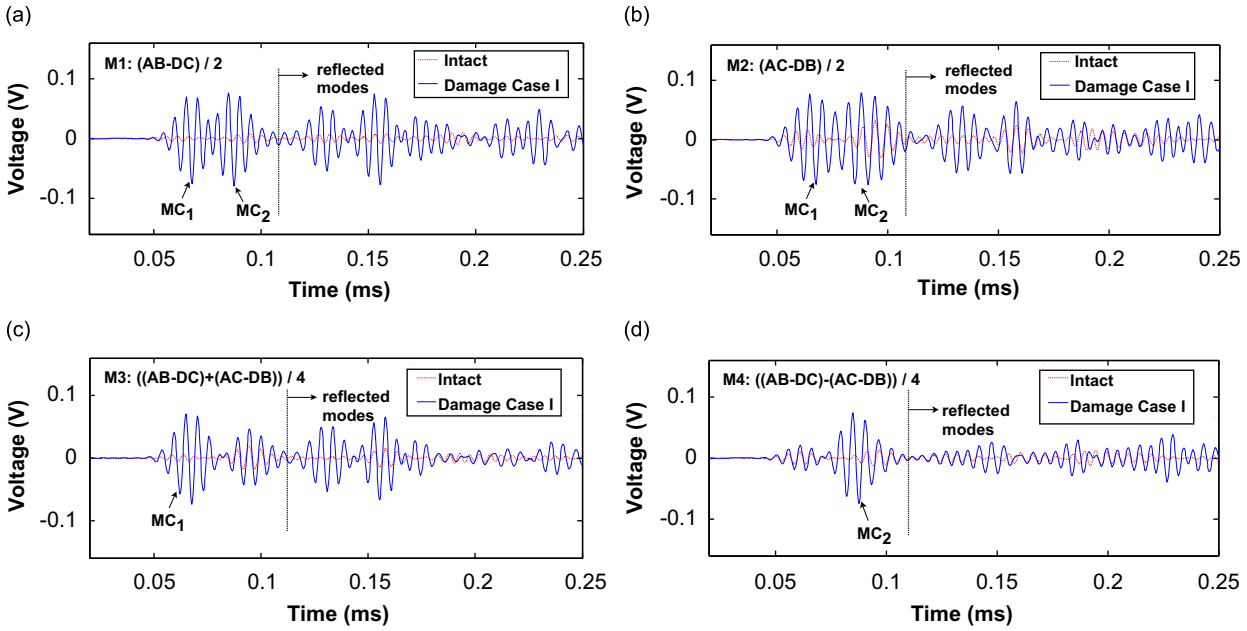

Fig. 8. Comparison of signals M1–M4 obtained from the intact and Damage Case I (at 180 kHz): (a) signal M1 given by (AB − DC)/2; (b) signal M2 given by (AC − DB)/2; (c) signal M3 given by {(AB − DC) + (AC − DB)}/4; and (d) signal M4 given by {(AB − DC) − (AC − DB)}/4.

be noted that there are additional converted modes in the reflected regions of all signals and it is difficult to identify each of them.

Fig. 9(a) shows the corresponding transfer-impedances of signals M1–M4. Then, the average energies for transfer impedances were computed in Fig. 9(b), and instantaneous damage diagnosis was subsequently performed on them as

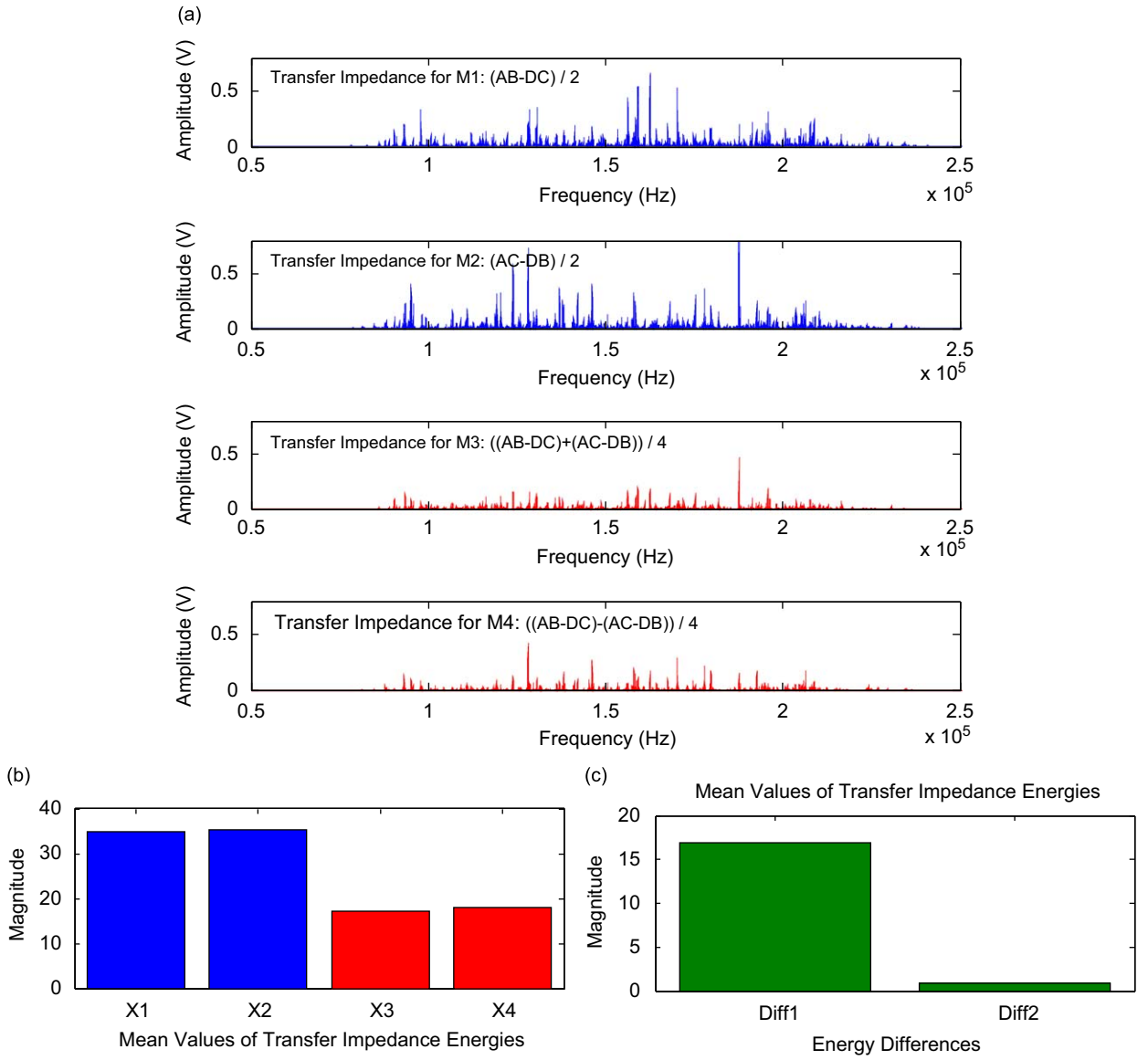

Fig. 9. Instantaneous damage diagnosis using the averaged transfer impedance energies of signals M1–M4 obtained from Damage Case I: (a) transfer impedances of signals M1–M4 obtained from Damage Case I of the plate; (b) averaged transfer impedance energies ($X1$, $X2$, $X3$ and $X4$) of signals M1–M4; and (c) since Diff 1 > Diff 2, the plate is diagnosed as in its damaged condition.

displayed in Fig. 9(c). It should be noted that the overall energy level of Damage Case I shown in Fig. 9(b) is much higher than that of the intact case shown in Fig. 6(b). Furthermore, it is observed that the energy ratio of Class A transfer impedances to Class B impedances tends to be close to 2:1. Since 'Diff 1' is larger than 'Diff 2' in Fig. 9(c), the presence of damage is instantaneously identified.

4.3. Damage Case II: crack behind one of the PZTs

In this subsection, Damage Case II shown in Fig. 7(b) has been investigated. A crack of the same size ($40 \times 1 \times 3\,\text{mm}^3$) as the previous example was introduced 60 mm behind PZT A. Then, converted modes, MC_1 and MC_2, would appear as part of signals reflected from one of the boundaries close to PZT A rather than as part of direct path signals between the first arrivals of the S_0 and A_0 modes. The same procedure as described in Sections 4.1 and 4.2 was repeated for the composition of M1–M4, calculation of transfer impedances, and damage classification. The average energies of the proposed transfer impedances were computed in Fig. 10(a), and instantaneous damage diagnosis was performed as in Fig. 10(b). It is observed that the energy ratio tends to be near "2:1" between Class A transfer impedances (for the first two) and Class B impedances

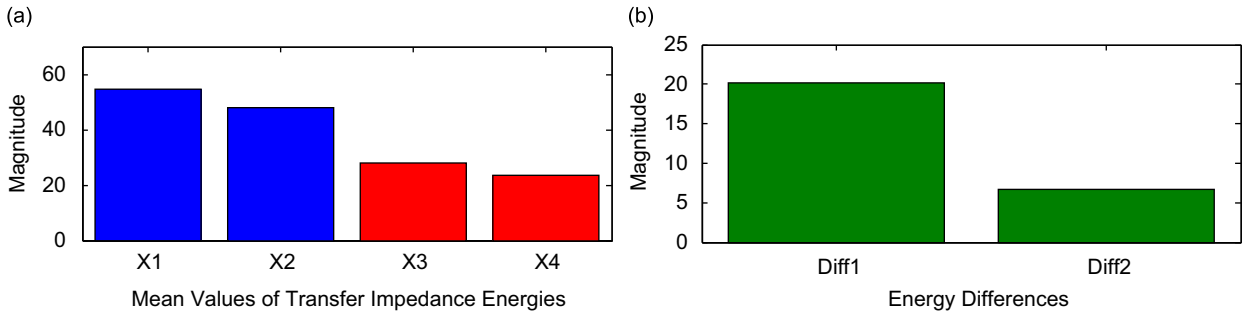

Fig. 10. Instantaneous damage diagnosis using the averaged transfer impedance energies of signals M1–M4 obtained from Damage Case II: (a) averaged transfer impedance energies ($X1$, $X2$, $X3$ and $X4$) of signals M1–M4 and (b) since Diff 1 > Diff 2, the plate is diagnosed as in its damaged condition.

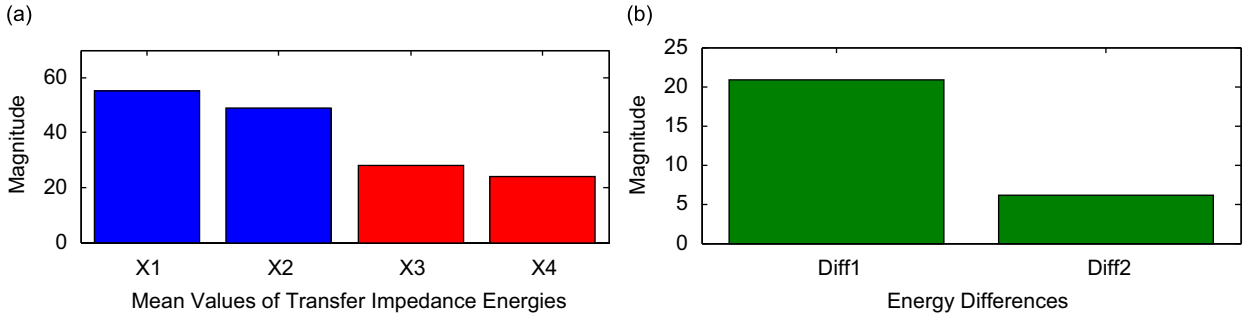

Fig. 11. Instantaneous damage diagnosis using the averaged transfer impedance energies of signals M1–M4 obtained from Damage Case III: (a) averaged transfer impedance energies ($X1$, $X2$, $X3$ and $X4$) of signals M1–M4 and (b) since Diff 1 > Diff 2, the plate is diagnosed as in its damaged condition.

(for the last two). Subsequently, the condition of the specimen has been instantaneously diagnosed as "Damaged Condition", since 'Diff 1' is larger than 'Diff 2'. Note that the proposed frequency-domain approach provides robust crack diagnosis even when the converted modes appear as part of the reflected signals.

4.4. *Damage Case III: crack out of the direct wave path (side)*

As the third damage case, a crack of the same size as before was introduced between PZTs A and B but off the direct wave path, as shown in Fig. 7(c). Here, the crack is carefully oriented and positioned so that the converted modes need to be reflected from the boundaries several times before they can measured at PZT B. The same procedures as described in Sections 4.1 and 4.2 were repeated for the composition of M1–M4, calculation of transfer impedances, and damage classification. It is noted that the identification of both mode conversions and fundamental modes becomes challenging in the time-domain. The average energies of the transfer impedances described in Section 3.2 were computed in Fig. 11(a), and instantaneous damage diagnosis was shown in Fig. 11(b). Again, it is observed that the energy ratio tends to be near "2:1" between Class A (for the first two) and Class B (for the last two). The results in Fig. 11 indicate that the condition of the specimen has been instantaneously diagnosed as "Damaged Condition", since 'Diff 1' is larger than 'Diff 2'. It is, therefore, confirmed that the proposed frequency-domain approach provides robust crack detection results regardless of crack locations and orientations.

4.5. *Damage Case IV: multiple cracks*

As the final damage case, two cracks of the same size of $40 \times 1 \times 3\,\mathrm{mm}^3$ were introduced along and out of the direct wave path, as shown in Fig. 7(d). It can be expected that multiple mode conversions occur not only when Lamb waves propagate along the direct path but also when reflected from boundaries. The average energies for the transfer impedances were computed in Fig. 12(a) and instantaneous damage diagnosis result was subsequently reported in Fig. 12(b). All the results in Fig. 12 were consistent with the ones from the previous damage cases. Furthermore, the magnitudes of the averaged transfer impedance energies for Damage Cases IV (Fig. 12) were larger than those from the previous Damage Cases I–III (Figs. 9–11). It can be, therefore, confirmed that the proposed reference-free damage detection technique works well even in the presence of multiple cracks regardless of the crack locations and orientations.

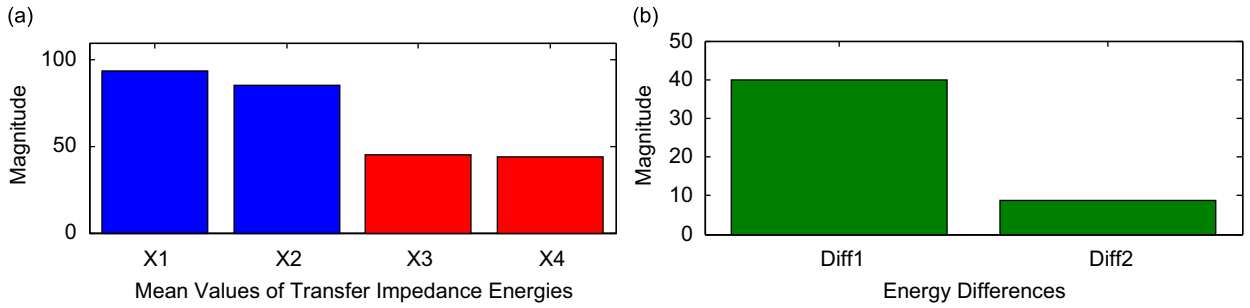

Fig. 12. Instantaneous damage diagnosis using the averaged transfer impedance energies of signals M1–M4 obtained from Damage Case IV: (a) averaged transfer impedance energies (X1,X2, X3 and X4) of signals M1–M4 and (b) since Diff 1 > Diff 2, the plate is diagnosed as in its damaged condition.

5. Conclusions

In this study, a reference-free crack detection technique has been developed for plate structures so that crack formation could be identified using transfer impedances between pitching and catching PZTs. This transfer impedance technique advances the previously developed time-domain technique so that mode conversion produced by a crack formation can be detected in the frequency-domain rather than in the time-domain. In the previous time-domain approach, individual Lamb wave modes such as S_0, A_0 and converted modes should be decomposed and identified in the time-domain. However, these procedures can be complicated when the crack is not directly along the wave path and there are multiple reflections and additional higher modes. Furthermore, extra caution is required to determine several design parameters during experiments. For instance, an optimal driving frequency needs to be selected after examining a Lamb wave tuning curve and the truncation time point should be carefully decided for signal collection.

The proposed frequency-domain approach, on the other hand, does not require the selection of a single optimal driving frequency or the decomposition of individual Lamb modes, since it only considers the crack-induced energy increase over some frequency range. Furthermore, since only the overall energy increase produced by mode conversion is concerned, the proposed technique is less responsive to the driving frequency range and the length of each time signal. Another advantage of this study is that not only a single crack but also multiple cracks can be detected even when the crack(s) is (are) not along a direct wave path. The validity of the proposed frequency-domain approach has been tested through a series of laboratory experiments using aluminum plates with a uniform thickness. From the experiments, it has been confirmed that this improved reference-free technique could be successfully utilized to identify cracks regardless of their location, orientation, and number. However, the proposed frequency-domain technique only identifies the existence of damage and does not locate the damage. Currently, other issues such as temperature variation and structural complexities on reference-free damage detection are also being investigated.

Acknowledgments

This research is supported by the Radiation Technology Program under Korea Science and Engineering Foundation (KOSEF) and the Ministry of Science and Technology (M20703000015-07N0300-01510), by the Grant (06KLSGC01) from Cutting-edge Urban Development-Korean Land Spatialization Research Project funded by Ministry of Land, Transport and Maritime Affairs, and by Applied Research Grant from the Agency for Defense Development (UC080019JD). Any opinions, findings, and conclusions or recommendations expressed in this material are those of the authors and do not necessarily reflect the views of the funding agencies.

References

[1] S. Park, C.-B. Yun, Y. Roh, Active sensing-based real-time nondestructive evaluations for steel bridge members, *KSCE, Structural Engineering* 10 (1) (2006) 33–39.
[2] H. Sohn, Effects of environmental and operational variability on structural health monitoring, *Philosophical Transaction of the Royal Society of London A* 365 (2007) 539–560.
[3] J.M. Nichols, M. Seaver, S.T. Trickey, A method for detecting damage-induced nonlinearities in structures using information theory, *Journal of Sound and Vibration* 297 (1–2) (2006) 1–16.
[4] E.S. Sazonov, P. Klinkhachom, U.B. Halabe, H.V.S. GangaRoa, Non-baseline detection of small damages from changes in strain energy mode shapes, *Nondestructive Testing and Evaluation* 18 (3–4) (2002) 91–108.
[5] H. Sohn, H.W. Park, K.H. Law, C.R. Farrar, Combination of a time reversal process and a consecutive outlier analysis for baseline-free damage diagnosis, *Journal of Intelligent Material Systems and Structures* 18 (2007) 335–346.
[6] S.B. Kim, H. Sohn, Instantaneous reference-free crack detection based on polarization characteristics of piezoelectric materials, *Smart Materials and Structures* 16 (2007) 2375–2387.
[7] J. Fraden, *Handbook of Modern Sensors*, American Institute of Physics, New York, 2001.

[8] R.C. Buchanan, *Ceramic Materials for Electronics*, Dekker, New York, 1986.
[9] V. Giurgiutiu, Tuned Lamb wave excitation and detection with piezoelectric wafer active sensors for structural health monitoring, *Journal of Intelligent Material Systems and Structures* 16 (2005) 291–305.
[10] Y. Cho, Estimation of ultrasonic guided wave mode conversion in a plate with thickness variation, *IEEE Transaction on Ultrasonics, Ferroelectric and Frequency. Control* 47 (2000) 591–603.
[11] I. Viktorov, *Rayleigh and Lamb Waves*, Plenum, New York, 1967.
[12] Z. Su, L. Ye, Selective generation of Lamb wave modes and their propagation characteristics in defective composite laminates, *Journal of Material Des. Applied L* 218 (2004) 95–110.
[13] K. Yamanaka, Y. Nagata, T. Koda, Selective excitation of single-mode acoustic waves by phase velocity scanning of a laser beam, *Applied Physics Letter* 58 (1991) 1591–1593.
[14] P.D. Wilcox, M.J.S. Lowe, P. Cawley, Mode and transducer selection for long range Lamb wave inspection, *Journal of Intelligent Material Systems and Structures* 12 (2001) 553–565.